7898

J. Am. Chem. Soc. **1985**, *107*, 7898–7904

g Tensor in Low-Spin Heme Systems Using Molecular Orbital Theory—Ferricytochrome *c* and Nitrosylhemoglobin[†]

K. C. Mishra, Santosh K. Mishra, J. N. Roy, S. Ahmad, and **T. P. Das***

Contribution from the Department of Physics, State University of New York at Albany, Albany, New York 12222. Received July 23, 1984

Abstract: The **g** tensors for the low-spin heme proteins ferricyclochrome *c* and nitrosylhemoglobin are investigated by studying the perturbation effect of spin–orbit interactions with molecular orbital wave functions and energy levels utilized earlier for the study of hyperfine interactions in these systems. While the major contributions to the shifts in the tensor components from the free-electron value, *g* = 2.0023, arise from excitations to and from the unpaired spin state from occupied or empty states, respectively, involving substantial iron d-orbital character, significant contributions are also found from excitations involving other states. The latter effect would not be included in a crystal field treatment of the **g** tensor. Another effect which would not be included in a crystal field treatment, namely the influence of spin–orbit interactions from ligand atoms, is found to be rather small. Our analysis provides reasonable agreement between the theoretical and experimental principal **g**-tensor components in the two molecules, both with respect to magnitudes and orientations. The remaining differences are used to draw conclusions regarding the accuracies of the electronic wave functions and energy levels used in our investigations. Additional mechanisms that could contribute to the g-shift tensor, besides the perturbation effect of spin–orbit interaction that is conventionally used, are discussed.

I. Introduction

The **g** tensors in biological systems like hemoglobin derivatives provide valuable insights into the nature of the valence orbitals and their relative spacings with respect to each other. The quantitative analysis for the origin of the **g** tensor has usually been carried out[1,2] by crystal field theory which deals with only the valence orbitals that have mainly 3d character, approximating them as purely 3d orbitals. Using perturbation theory for the combined influence of spin–orbit and orbit–magnetic field interactions in determining the net splitting of the M_s (spin magnetic quantum number) states in spin $^1/_2$ system to fit experimental data, one derives useful semiquantitative information regarding the strengths of the cubic, axial, and rhombic components of the crystal field. The assumption of localized 3d orbitals on iron is, however, inadequate to explain the hyperfine interactions of ligand ^{14}N nuclei[3] as well as protons in the protoporphyrin ring[4] which have been studied by ENDOR and NMR techniques. For these nuclei, molecular orbital wave functions have been shown to be successful in explaining the observed hyperfine interactions in a number of high-[5] and low[6]-spin hemoglobin derivatives. We felt therefore that, as part of our continuing program of trying to explain magnetic and hyperfine properties of hemoglobin derivatives, it would be interesting to study **g** tensors using molecular orbital theory. For our investigations, we have chosen the two systems ferricytochrome *c* (ferricyt *c*) and nitrosylhemoglobin (NOHb) where in earlier work[6] the hyperfine interactions of the ligand nuclei ^{14}N and protons were successfully analyzed by using molecular wave functions obtained by the self-consistent charge extended Hückel (SCCEH) procedure.[7] The occupied and excited state wave functions and energies in these molecules were utilized in the perturbation calculation of **g** tensors.[8]

A molecular orbital treatment of the **g** tensor has recently been used[9] for nitrosyl hemoglobin. However, there is a difference in motivation between this earlier analysis[9] and that in the present paper.[7] In the earlier investigation,[9] the extent of mixing of iron and ligand atom orbitals is estimated by using molecular orbitals with adjustable parameters and obtaining these parameters by fitting the **g** tensor and ^{14}N hyperfine data. In the present work, on the other hand, electronic energy levels and wave functions are used from ab initio investigations[6] to evaluate the components of the **g** tensor and compared with experiment. From the comparison with experiment one attempts to draw conclusions about the accuracy of the wave functions and energy levels and other mechanisms besides the perturbation of the valence electron

molecular orbital states by the spin–orbit interaction that is commonly considered.[8]

In section II, the perturbation procedure for the components of the **g** tensor in terms of molecular orbital theory will be briefly described. Section III presents the results of the **g** tensor in both nondiagonal forms with respect to the molecular axis as well as in diagonal forms in the principal axis systems. This section also compares our results with experiment and presents a discussion of further improvements in the theory that are suggested by the present work.

II. Theory

As pointed out earlier, theoretical treatments of the g-shift tensor in low-spin hemoglobin derivatives have usually been carried out within the framework of the crystal field approach.[1,2] In our present work, we have used a molecular orbital treatment.[8] It is therefore important to present a brief formulation of the appropriate theory so as to be able to discuss some points that are characteristic of the present approach. These include the roles of the molecular orbital wave functions and energies and of spin–orbit effects associated with ligand atoms in addition to the iron atom spin–orbit effect which is considered in crystal field theory.

In the perturbation treatment of the **g** tensor, one starts with the Hamiltonian

(1) Pilbrow, J. R.; Lowrey, M. R. *Rep. Prog. Phys.* **1980**, *43*, 433–495.
(2) Griffith, J. S. In "Theory of Transition Metal Ions"; Cambridge University Press: New York, 1964. Peisach, J.; Blumberg, W.; Adler, A. *Ann. Acad. Sci.* **1973**, *206*, 310–327.
(3) Scholes, C. P.; Van Camp, H. L. *Biochem. Biophys. Acta* **1976**, *434*, 290–296. Mulks, C. F.; Scholes, C. P.; Dickinson, L. C.; Lapidot, A. *J. Am. Chem. Soc.* **1979**, *101*, 1645–1654.
(4) Davis, D. G.; Charache, S.; Ho, C, *Proc. Natl. Acad. Sci. U.S.A.* **1969**, *63*, 1403–1409.
(5) Mallick, M. K.; Mun, S. K.; Mishra, S. L.; Chang, J. C.; and Das, T. P. *J. Chem. Phys.* **1978**, *68*, 1462–1473. Mun, S. K.; Mallick, M. K.; Mishra, S. L.; Chang, J. C.; Das, T. P. *J. Am. Chem. Soc.* **1981**, *103*, 5024–5031.
(6) Mun, S. K.; Chang, J. C.; Das, T. P. *Proc. Natl. Acad. Sci. U.S.A.* **1979**, *76*, 4842–4846. Mishra, K. C.; Mishra, S. K.; Das, T. P. *J. Am. Chem. Soc.* **1983**, *105*, 7729–7735.
(7) Hoffman, R. *J. Chem. Phys.* **1963**, *39*, 1397–1412. Zerner, M.; Gouterman, M.; Kobayashi, H. *Theor. Chim. Acta* **1966**, *6*, 363–400. Han, P. S.; Rettig, M. F.; Das, T. P. *Theor. Chim. Acta* **1970**, *16*, 1–21.
(8) Carrington, A.; McLachlan, A. D. In "Introduction to Magnetic Resonance"; Harper & Row: New York, 1963; Chapter 9.
(9) Doetschman, D. C. *Chem. Phys.* **1980**, *48*, 307–314. Doetschman, D. C.; Schwartz, S. A.; Utterback, S. G. *Chem. Phys.* **1980**, *49*, 1–8. Utterback, S. G.; Doetschman, D. C.; Szumowski, J.; Rizos, A. K. *J. Chem. Phys.* **1983**, *78*, 5874–5880.

g Tensor in Low-Spin Heme Systems

J. Am. Chem. Soc., Vol. 107, No. 26, 1985 7899

$$\mathcal{H} = \mathcal{H}_0 + \mathcal{H}_{so} + \mathcal{H}_M \qquad (1)$$

for electrons in a magnetic field. In eq 1, $\mathcal{H}_0$ corresponds to the unperturbed Hamiltonian, including the kinetic and potential energy terms for the many-electron molecular system. The terms $\mathcal{H}_{so}$ and $\mathcal{H}_M$ represent respectively the spin–orbit interaction and the Zeeman interaction between the electrons and the applied field. For an electronic system with total orbital angular momentum, $\vec{L}$, and spin angular momentum, $\vec{S}$, $\mathcal{H}_M$ can be written as

$$\mathcal{H}_M = \beta\vec{H}\cdot(\sum_i \vec{l}_i + g_e\sum\vec{s}_i) \qquad (2)$$

where $\vec{l}_i$ and $\vec{s}_i$ denote the orbital and spin angular momentum operators for the electron i and the summation on i is carried over all the electrons, β represents the Bohr magneton, and $g_e = 2.0023$, the g factor for the electrons. The origin for the orbital angular momenta $\vec{l}_i$ can be chosen arbitrarily and determines the gauge adopted for the magnetic vector potential corresponding to the applied field.[10]

In the analysis of electron paramagnetic resonance measurements, the Zeeman interaction is taken in the form

$$\mathcal{H}_{spin} = \beta\vec{H}\cdot\hat{g}\cdot\vec{S} \qquad (3)$$

in the spin-Hamiltonian, $\vec{S}$ representing the effective spin of the system which for a spin $^1/_2$ system is the total spin and $\hat{g}$ is the **g** tensor. If one ignores the spin–orbit interaction, then the orbital angular momentum is completely quenched, and $\hat{g}$ is isotropic and equal to g_e, the free-electron value. However, the spin–orbit interaction Hamiltonian, $\mathcal{H}_{so}$, will unquench some of the orbital angular momentum and make the **g** tensor different from g_e.

The first step in evaluating the **g** tensor is to obtain the many-electron wave functions for the total spin state $\Psi_{\pm}$, corresponding to $M_s = \pm^1/_2$, in the presence of spin–orbit interaction, using perturbation theory. These wave functions are given by

$$\Psi_{\pm} = \Psi_{0,\pm1/2} + \sum_{n,M_s} \frac{\langle \Psi_{n,M_s}|\mathcal{H}_{so}|\Psi_{0,\pm1/2}\rangle}{E_0 - E_n}\Psi_{n,M_s} \qquad (4)$$

where $\Psi_{0,\pm1/2}$ and Ψ_{n,M_s} refer to the ground and excited many-electron eigenfunctions of $\mathcal{H}_0$. The eigenfunctions Ψ_{n,M_s} and eigenvalues E_n for the multielectron system were obtained by using the SCCEH procedure, M_s, corresponding to the magnetic quantum number. The functions Ψ_{n,M_s} are expressed in determinational forms in terms of the one-electron molecular orbitals ϕ_{μ,M_s} as:

$$\Psi_{n,M_s} = \text{Det } |\phi_{1,M_s}^{(1)}, ...,\phi_{n,M_s}^{(n)}| \qquad (5)$$

The molecular orbitals (MO) ϕ_{μ,M_s} in eq 5 are usually expressed as linear combination of atomic orbitals (LCAO), χ_{i,M_s} in the form

$$\phi_{\mu,M_s} = \sum C_{\mu i}\chi_{i,M_s} \qquad (6)$$

The LCAO coefficients $C_{\mu i}$ and molecular energies ϵ_{μ} are obtained as usual by solving the secular equations

$$\text{Det } |\mathcal{H}_{ij} - \epsilon_{\mu}S_{ij}| = 0 \qquad (7)$$

derived from linear equations for the $C_{\mu i}$. In eq 7, $\mathcal{H}_{ij}$ and S_{ij} are the Hamiltonian and overlap matrix elements in the basis χ_{i,M_s}. In the SCCEH procedure, one uses semiempirical approximations for the diagonal and off-diagonal matrix elements $\mathcal{H}_{ii}$ and $\mathcal{H}_{ij}$ involving for $\mathcal{H}_{ii}$ the ionization energies and Mulliken charges[11] based on the $C_{\mu i}$ and for $\mathcal{H}_{ij}$, the Wolfsberg–Helmholtz approximation.[7]

The formulation of the spin–orbit Hamiltonain $\mathcal{H}_{so}$ is in general rather complicated for a multicenter problem.[12] However, since the spin–orbit effect for each atom is rather short-ranged, varying

(10) Chan, S. I.; Das, T. P. *J. Chem. Phys.* **1962**, *37*, 1572–1533.
(11) Mulliken, R. S. *J. Chem. Phys.* **1955**, *23*, 1833–1841.
(12) Sharma, R. R.; Das, T. P.; Orbach, R. *Phys. Rev.* **1968**, *171*, 378–388. Han, P. S.; Das, T. P.; Rettig, M. F. *J. Chem. Phys.* **1972**, *56*, 3861–3873.
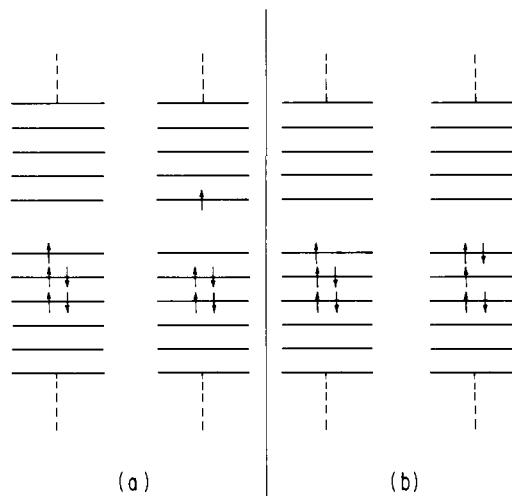
Figure 1. Schematic representation of the two types of excitations that can contribute to the perturbation term in eq 10.

in an hydrogenic approximation as r_A^{-3} with respect to the distance r_A from a nucleus A, one does not expect[12] ay two-center matrix elements of $\mathcal{H}_{so}$ to be so important. Consequently, one can write to a good approximation[8]

$$\mathcal{H}_{so} = \sum\zeta_A\vec{l}_{iA}\cdot\vec{s}_i \qquad (8)$$

where ζ_A is the spin–orbit constant corresponding to atom A and $\vec{l}_{iA}$ is the angular momentum centered about the nucleus of A.

To evaluate the components of $g_{\alpha\beta}$ of the **g** tensor, we use the equation[8]

$$\langle\Psi_{\pm}|\mathcal{H}_{spin}|\Psi_{\pm}\rangle = \langle\Psi_{\pm}|\mathcal{H}_M|\Psi_{\pm}\rangle \qquad (9)$$

Taking the diagonal matrix elements on both sides in eq 9, one obtains the diagonal components $g_{\alpha\alpha}$ ($\alpha = x, y, z$) considering the magnetic field to be applied in the α direction. The nondiagonal matrix elements in eq 9 give the nondiagonal components $g_{\alpha\beta}$ of the **g** tensor. By this procedure, after some manipulations, one gets the general expression

$$g_{\alpha\beta} = g_e\delta_{\alpha\beta} \pm 2\sum_n \frac{\langle\Psi_{0,M_s}|\sum_i l_{i\alpha}|\Psi_{n,M_s}\rangle\langle\Psi_{n,M_s}|\sum_{A,i}\zeta_A l_{iA\beta}|\Psi_{0,M_{s'}}\rangle}{E_0 - E_n} \qquad (10)$$

where the two signs in the second term on the right-hand side refer to two different modes of excitation and $M_s = M_s \pm 1$, the choice being determined by β and M_s. The positive sign is associate with excitations of the unpaired spin electron to higher states that are empty (fig. 1a) leading to decrease in the **g** factor from free-electron value, while the negative sign refers to excitations of electrons of antiparallel spin from the lower occupied states to the unpaired spin level (Figure 1b), leading to positive **g** shifts.

On using eq 5 for the many-electron wave functions Ψ_{0,M_s} and Ψ_{n,M_s} and eq 6 for the MO wave functions expressed as LCAO, eq 10 takes the form

$$g_{\alpha\beta} =$$

$$g_e\delta_{\alpha\beta} \pm 2\sum_n \sum_{ijkl} \frac{C_{\mu i}^{(0)}C_{\nu j}^{(n)}C_{\nu k}^{(n)}C_{\mu l}^{(0)}\langle\chi_i|l_{i\alpha}|\chi_j\rangle\langle\chi_k|\sum_A\zeta_A l_{A\beta}|\chi_l\rangle}{E_0 - E_n} \qquad (11)$$

in terms of matrix elements based on the atomic orbitals. In eq 11, the indices μ and ν in the LCAO coefficients $C_{\mu i}^{(0)}$, $C_{\nu i}^{(n)}$, ... refer to the MO of the states between which excitation occurs in going from the multielectron states Ψ_{0,M_s} and $\Psi_{0,M_{s'}}$ to the excited state Ψ_{n,M_s}. Thus, for the positive sign in eq 10 (Figure 1a), the $C_{\mu i}^{(0)}$ and $C_{\mu l}^{(0)}$ refer to the unpaired spin orbital from which the electron is excited to the higher empty state with the corresponding LCAO coefficients $C_{\nu j}^{(n)}$ and $C_{\nu k}^{(n)}$. For the negative sign (Figure 1b), $C_{\mu i}^{(0)}$ and $C_{\mu l}^{(0)}$ refer to the lower antiparallel spin state from

7900 *J. Am. Chem. Soc., Vol. 107, No. 26, 1985*

Mishra et al.
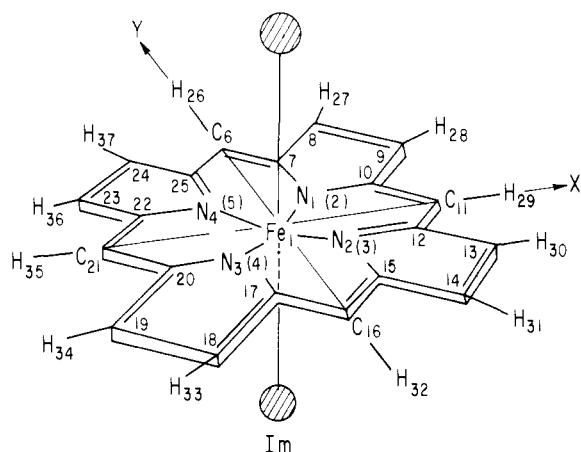
Figure 2. Model system used for the ferricytochrome *c* molecule showing the atoms in the porphyrin base. For the porphyrin nitrogens the numbers in parentheses refer to the atom numbers in ref 14 and the suffixes for all the atoms corresponding to the usual notation in the literature. The imidazole (Im) and methionine ligands are shown by the crossed circles.

which an electron is excited to the unpaired spin (antiparallel) state.

The energy denominators in eq 4, 10, and 11 all refer to the energy difference between the multielectron ground (Ψ_{0,M_s}) and excited (Ψ_{n,M_s}) states. If one were using a rigorous Hartree–Fock theory, then the total energy, E_0, would be given by

$$E_0 = \sum_\mu \epsilon_\mu - \sum_{\mu>\omega}(J_{\mu\omega} - K_{\mu\omega}) \qquad (12)$$

where μ and ω refer to the occupied one-electron states. In eq 12, the ϵ_μ are one-electron energies for states μ and $J_{\mu\omega}$ and $K_{\mu\omega}$, the Coulomb and exchange energies involving states μ and ω. An analogous expression holds for E_n, with i and j corresponding to the occupied one-electron states in the multielectron state Ψ_{n,M_s}. Thus in Hartree–Fock theory, we would have for ($E_0 - E_n$), corrections to the one-electron energy difference ($\epsilon_\mu - \epsilon_\nu$) involving the changes in Coulomb and exchange energies associated with electrons in states μ and ν. However, as discussed in earlier work[13] dealing with the related experimental parameter *D*, referring to zero-field splitting in high-spin states, it is not quite clear how much of the Coulomb and exchange interaction energies are involved in the ϵ_μ, which makes it uncertain whether one should subtract the total Coulomb and exchange energies as in the second term in eq 2 or use a fraction of the difference. In our present work, in the case of ferricyt *c*, the orbitals μ and ν that make the dominant contribution to the summation in eq 11 are very similar to each other, which makes the Coulomb and exchange energy corrections to the energy difference rather small. In the case of NOHb, the one-electron energy differences between the states that make significant contributions in eq 11 are rather substantial, which would also make the Coulomb and exchange energy corrections unimportant. We have, therefore, chosen to replace ($E_0 - E_n$) by ($\epsilon_\mu - \epsilon_\nu$). The effects of this approximation on our results for the **g** tensor will be discussed further in section III.

III. Results and Discussion

a. Ferricytochrome *c*. Before presenting our results for ferricyt *c*, we would like to briefly summarize the experimental **g** tensor data in this molecule from single crystal electron paramagnetic resonance (EPR) measurements[14] at 4 K. The principal components (g_1, g_2, g_3) of the **g** tensor were found to be 1.25, 2.25, and 3.06, respectively. The principal axis corresponding to the largest component g_3 was found to lie within 5° of the heme normal while the g_1 and g_2 components were close to the Fe–N$_1$ and Fe–N$_2$ directions (Figure 2), making angles of 4° and 5°,

(13) Han, P. S., in ref 12.
(14) Mailer, C.; Taylor, C. P. S. *Can. J. Biochem.* **1972**, *50*, 1048–1055.

Figure 3. The five d-like levels in ferricytochrome *c* that make important contributions to the perturbation expression in eq 11. The energies and eigenfunctions corresponding to these levels are included for reference.

respectively, with these directions.

For our **g**-tensor investigations using eq 11, we have made use of molecular orbitals obtained from SCCEH calculations that were utilized earlier[15] for the interpretation of hyperfine interaction of ^{14}N and ^{1}H nuclei from ENDOR measurements.[16,17] The structural arrangement used for iron and its ligands in this earlier work was taken from available X-ray data.[18] The pertinent eigenvectors making dominant contributions to the perturbation expression in eq 11 are listed beside the appropriate energy levels in Figure 3, which also lists the energy separations between these levels. We shall use terms like d_{xy}-like and d_{xz}-like henceforth to designate orbitals that have the largest coefficients in their MO for the d_{xy} and d_{xz} orbitals, respectively. In handling the contributions from orbitals of this type to the **g** tensor in eq 11, the entire MO functions including all other admixed d orbitals and ligand orbitals will be employed. The lowest of the orbitals shown in Figure 3 has primarily $d_{x^2-y^2}$ character while the next to highest one has primarily d_{xy} character, which is different from the usual convention. This is a consequence of our choice of X and Y axes in Figure 2. If these axes had instead been chosen to correspond to Fe–N$_1$ and Fe–N$_2$ directions, respectively, then the $d_{x^2-y^2}$-type and d_{xy}-type orbitals would have been interchanged to correspond to the standard convention. Although we have only shown the five orbitals with substantial d characters, we have included in our summation in eq 11 contributions from all occupied and unoccupied orbitals having any significant d character. The significant departure of the coefficients for the d-orbital components from unity in the expression for the wave function in Figure 3 is indicative of the strong covalent bonding between the iron atom and its surroundings. This strong bonding is also manifested by the small effective charge 0.2390 on the iron and the fact that only about 65% of the unpaired spin population resides[15] on the iron atom. The migration of some of the spin population to the neighboring atoms is manifested by the fact that significant ^{14}N and ^{1}H hyperfine interactions are observed[16,17] for this molecule. The satisfactory agreement we have obtained[15] between theory and experiment[16,17] for these hyperfine interactions lends support to the correctness of the calculated electron distributions in this molecule. Because of this significant delocalization of the orbitals, we have examined the contribution to the components of the **g** tensor from the spin–orbit effect associated with the ligand nitrogen atoms by including the effects of these atoms in the summation over A in eq 11. Their contribution was, however, found to be only about 1% of that due to the iron atom, both because the spin–orbit coupling constant ζ was about a factor of 4 smaller than in iron[8] (410 cm^{-1}) and that only part of the spin population (totalling 0.35) moving out[15] from iron appeared on the nitrogen ligands.

Using the procedure outlined in section II leading to eq 11, together with our calculated energy levels and electronic wave functions, we have obtained the **g** tensor shown in eq 13 for the coordinate system in Figure 2:

(15) Mishra, K. C., in ref 6.
(16) Scholes, C. P., in ref 3.
(17) De Beer, R., private communication.
(18) Dickerson, R. E.; Takano, T.; Eisenberg, D.; Kallai, O. B.; Samson, L.; Cooper, A.; Margoliash, E. *J. Biol. Chem.* **1971**, *246*, 1511–1535. Salemme, F. R.; Freer, S. T.; Xuong, Ng. H.; Alden, R. A.; Kraut, J. *J. Biol. Chem.* **1973**, *248*, 3910–3921. Salemme, F. R.; Kraut, J.; Kamen, M. D. *J. Biol. Chem.* **1973**, *248*, 7701–7716.

g *Tensor in Low-Spin Heme Systems*

J. Am. Chem. Soc., Vol. 107, No. 26, 1985 7901

$$\hat{g} = \begin{pmatrix} 3.6959 & -0.0690 & 0.1682 \\ -0.0690 & 2.4438 & 0.0529 \\ 0.1682 & 0.0529 & 2.0351 \end{pmatrix} \qquad (13)$$

the order of the rows and column being $(Z, X, \text{and } Y)$. From eq 13, it can be seen that the component g_{zz} is the largest one, deriving the dominant contribution to its difference from the free-electron **g** value from excitations of the type in Figure 1b from the paired d_{xz}-like state in Figure 3. The small separation between these levels is responsible for the large shift from free-electron character in g_{zz}. The components g_{xx} and g_{yy} had relatively smaller shifts from the free-electron value, the shifts arising primarily again from excitations of the type in Figure 1b from the paired spin $d_{x^2-y^2}$-like state (Figure 3) to the unpaired spin d_{yz}-like state. The off-diagonal elements of the **g** tensor are small, but significant, and one has to diagonalize the tensor in eq 13 to obtain the principal components and the orientations of the principal axes. These are given in eq 14 and 15, the columns in eq 15 for the direction cosines $\gamma_{i'i}$ corresponding to the principal axes Z', X', and Y' and the rows to the axes Z, X, and Y in Figure 2. On comparing the results

$$g_{z'z'} = 3.7159, \quad g_{x'x'} = 2.4489, \quad g_{y'y'} = 2.0100 \qquad (14)$$

$$\gamma_{i'i} = \begin{pmatrix} 0.9939 & 0.0357 & -0.1039 \\ -0.0498 & 0.9894 & -0.1366 \\ 0.0979 & 0.1410 & 0.9852 \end{pmatrix} \qquad (15)$$

in eq 14 and 15 with experiment,[14] we find that as far as trends in the magnitudes of the principal components are concerned, there is good overall agreement between our results and experiment. Thus, the largest component $g_{z'z'}$ in eq 14 has the corresponding principal axis oriented close to the Z axis in Figure 2 and about 6° away, in good agreement with experiment. The other two principal axes X' and Y' lie close to the XY plane as observed experimentally,[14] making angles of about 8° each with the X and Y axes, respectively, which are smaller than the angles close to 40° from experiment. There are also sizable differences in magnitude between our principal components and those observed experimentally. In keeping with our aims for this work as mentioned at the outset in section I, which were to see how well one could explain the observed **g** tensors in hemoglobin derivatives using ab initio electronic wave functions and energy levels from SCCEH procedure and look for improvements that can provide agreement with experiment, we proceed to discuss possible sources for such improvements.

Thus, in eq 11, the numerator involves the wave functions for the occupied and unoccupied states while the denominator involves the corresponding energy differences. Since the electronic wave functions in ferricytochrome c have been found to provide satisfactory explanations[15] of the observed magnetic hyperfine interactions of the nuclei in this molecule,[16,17] the wave functions we have used, at least for the occupied states, are reasonably accurate. One can also assume that the excited-state wave functions are reliable as well, because the ground- and excited-state wave functions are obtained by the same procedure. This then puts the primary onus for the differences between the theoretical and experimental **g** tensor components on the energy denominators in eq 11. Thus, for $g_{z'z'}$, the departure of **g** shift from free-electron value is found theoretically to be about 1.71, as compared to the experimental result[14] of 1.06. Thus an increase in the small separation of the d_{xz}-like and d_{yz}-like levels by about 60% could bridge the gap between theory and experiment for $g_{z'z'}$. One of the sources that seems a likely candidate for increasing the energy separation between these two levels is the influence of spin–orbit interaction itself. In addition to producing a mixture of the wave functions for the d_{xz}- and d_{yz}-like states, which has resulted in the sizable shift in the **g** component from the free-electron **g** value, the spin–orbit interaction can also lead to significant shifts in the energy values for these levels. This is because their separation of about 0.03 eV (263 cm⁻¹), as seen from Figure 3, is small to start with, and of comparable order of magnitude as the effective spin–orbit matrix element of about 100 cm⁻¹ connecting them. We have evaluated the changes in energy for the two levels in second-order perturbation theory and find that the lower one is

depressed by 0.011 eV (87 cm⁻¹) with respect to its position in Figure 3, while the higher one is raised by the same amount. This leads to a modified separation between the two levels of 437 cm⁻¹, a change from the earlier value of the order needed to improve agreement of $g_{z'z'}$ with experiment. The use of the modified energy separation in the denominator in eq 11 for the d_{xz}- and d_{yz}-like states is equivalent to including the effect of spin–orbit interaction on the energy levels to all orders as is done in the literature on many-body perturbation theory.[19] We have employed the modified energies of the d_{xz}- and d_{yz}-like levels in obtaining all the components of the nondiagonal tensor **g** using eq 11. The replacement for eq 13 then comes out as

$$g = \begin{pmatrix} 3.0251 & -0.0368 & 0.1011 \\ -0.0368 & 2.3560 & 0.0402 \\ 0.1011 & 0.0402 & 2.0251 \end{pmatrix} \qquad (16)$$

On comparing eq 13 and 16, it can be seen that the components g_{zz}, g_{xz}, g_{yz} are the ones that are most influenced by the effect of spin–orbit interaction on the energy levels corresponding to the d_{xz}- and d_{yz}-like states. This is to be expected since the perturbation expression in eq 11 for these components derives major contribution from the excitation from the d_{xz}-like state in Figure 3 to the d_{yz}-like state. The other three components g_{xx}, g_{yy}, and g_{xy} do not derive any contribution from this excitation and are thus relatively less influenced by the effect of spin–orbit interaction on the energy levels for the d_{xz}- and d_{yz}-like levels. Whatever effect does occur for these latter components arises from the changes produced by the spin–orbit interaction in the relatively larger separations between the d_{yz}-like unpaired spin state and the paired state $d_{x^2-y^2}$ or the empty state d_{xy}.

On diagonalization, eq 16 leads to the principal components

$$g_{z'z'} = 3.0368, \quad g_{x'x'} = 2.3560, \quad g_{y'y'} = 2.0094 \qquad (17)$$

$$\gamma_{i'i} = \begin{pmatrix} 0.9940 & 0.0352 & -0.1027 \\ -0.0480 & 0.9909 & -0.1254 \\ 0.0974 & 0.2397 & 0.9868 \end{pmatrix} \qquad (18)$$

in place of the results in eq 14 and direction cosines replacing eq 15. The direction cosines and $g_{y'y'}$ are not significantly affected by the spin–orbit effect on the energy levels, but the components $g_{z'z'}$ and $g_{x'x'}$ are, the former more substantially than the latter, as would be expected from a comparison of the nondiagonal **g** tensor in eq 13 and 16. Both the components $g_{z'z'}$ and $g_{x'x'}$ are now in better agreement with experiment[14] than the values in eq 14. The $g_{y'y'}$ component, however, still differs substantially from experiment.

As a matter of fact, for the $g_{y'y'}$ tensor, while our result is close to the free-electron value or actually slightly larger, the experimental value[14] is substantially smaller. First, considering the question of theory giving a **g** factor slightly larger than the free-electron value, this situation can be traced to a competition between excitations of type (1a) and (1b) (Figure 1), the former arising primarily from excitation from the d_{yz}-like state to d_{xy}-like state and the latter from excitations both from the doubly occupied $d_{x^2-y^2}$-like state to d_{yz}-like as well as from some lower doubly occupied states that have small but significant d characters. Corrections to the energy separations between these various levels with respect to the d_{yz}-like level could alter the individual contributions to the **g** shift and change the latter from positive to negative. These corrections could arise from the facts that due to the semiempirical nature of the SCCEH procedure,[7] there may be inaccuracies in either the one-electron energy separation ($\epsilon_\mu - \epsilon_\nu$) or the effects of neglecting the direct and exchange energy differences in obtaining the difference ($E_o - E_n$) in the total energies for the ground and excited configurations in eq 11. For reasons mentioned in section II, one would expect the latter source to be less important than possible inaccuracies in ($\epsilon_\mu - \epsilon_\nu$). However, it is difficult to explain the observed $g_{x'x'}$, as small as 1.25, by purely a change in level spacings, and one has, perhaps,

(19) Chang, E. S.; Pu, R. T.; Das, T. P. *Phys. Rev.* **1968**, *174*, 1–16.
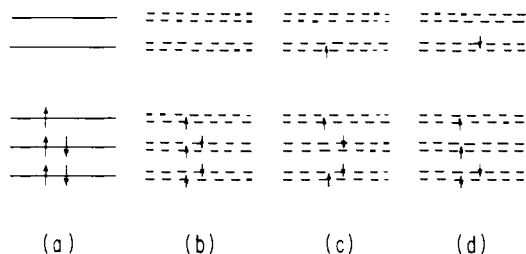
Figure 4. Representation of the nature of excitations contributing to the g-shift tensor when exchange polarization effects are considered. In part a are presented the levels before EP effects are included, as in RHF theory; part b represents the levels after EP effects are included, as in UHF theory, the degeneracy between the states with spins parallel and antiparallel to the spin in the unpaired level having been lifted; parts c and d represent excitations involving opposite spins from paired spin levels which would no longer produce cancelling contributions, as was the case before EP effects were included.

to look for other mechanisms besides the conventional spin–orbit mechanism considered in section II. Two such mechanisms that should be considered can be termed exchange polarization (EP) and Casimir mechanisms.

The EP mechanism can be understood by referring to Figure 4. It is based on the fact that through exchange interaction the paired spin levels corresponding to spin states parallel and antiparallel to the spin in the unpaired level would have different energies[20,21] and wave functions as shown in Figure 4b. This effect is usually neglected in conventional Hartree–Fock theory, unless one uses what is called in the literature the unrestricted Hartree–Fock (UHF) approach,[20] and has also been neglected in the SCCEH approach used here. In the UHF approach, however, excitations of the type in parts c and d in Figure 4 would not cancel, as they would have if the restricted Hartree–Fock type picture as in Figure 4a had been considered. This could lead to a significant contribution to g shift especially because all the paired spin levels can take part in this process. This would apply also to the core states of iron such as the 3p states for which the spin–orbit interactions would be particularly strong.

The Casimir mechanism is a relativistic one[22,23] and has been utilized[24] for zero-field splittings in transition-metal ions and related properties. It can be understood by noting that in relativistic theory,[23] the radial characters of the individual d states in isolated atoms and ions are different, which leads to a similar unquenching of angular momentum as is done by spin–orbit interaction. One thus has an additional mechanism to that represented by eq 11, involving directly the expectation value of the Zeeman term in eq 2 with use of relativistic wave functions, without requiring spin–orbit effect for unquenching as in eq 4.

These mechanisms would involve additional difficult computations but should be attempted in the future as well as possible improvements in the energy denominators in eq 11. Thus, it would be helpful to see if improvements in the SCCEH theory such as the incorporation[25,26] of Coulomb interactions between the electrons on an atom and the charges on its neighbors influence the one-electron energy difference $(\epsilon_\mu - \epsilon_\nu)$ significantly. It would also be desirable to study the energy differences $(E_o - E_n)$ in eq 11 by more first-principle methods such as the fully self-consistent Hartree–Fock theory[27–29] or the less time-consuming multiple

scattering-Xα procedure[30] using the local-density approximation[31] for exchange interactions. It will be interesting to see if the incorporation of these improvements and the influence of the EP and Casimir mechanisms can bridge the substantial gap between the theoretical values of $g_{y'y'}$ in eq 15 and experiment and the relatively smaller gap for $g_{x'x'}$ while leaving the good agreement for $g_{z'z'}$ unchanged.

Lastly, one would also have to consider the possibility of perturbations in the molecular orbital wave functions,[15] for the system involving the heme and its methionine and imidazole ligands, due to the influence of neighboring groups on the protein chains. These perturbations may lead to asymmetries in the wave functions and spin densities that could contribute to $g_{y'y'}$ in the direction for improved agreement with experiment.

Before concluding this discussion of our results for ferricytochrome c, we would like to point out that a crystal field type analysis[32] has been carried out in the literature on the g tensor in this system. It is difficult to make a quantitative comparison between our results and those of the crystal field analysis because of the different aims of the two investigations. Thus, the crystal field theory treatment involves[32] determination of a certain number of parameters, associated with the splitting of the t_{2g}-like levels and the influence of covalent bonding on the strength of the spin–orbit interaction, referred to as the orbital reduction effect, by making fits with the g-tensor data. Our approach, on the other hand, is one of using the unpaired spin, paired spin, and empty molecular orbitals from ab initio investigations to obtain the components of the g tensor for comparison with experiment and drawing conclusions from the nature of the agreement about the accuracy of the orbitals and the importance of other mechanisms. However, the crystal field analysis[32] does have some features that can be compared with the natures of the electronic states from our SCCEH investigations. One of these is the feature that the unpaired spin orbital is in a mixture of d_{yz}- and d_{xz}-like states, in agreement with the nature of this orbital from our SCCEH investigations. Secondly, the crystal field analysis[32] uses the assumption of relatively weak covalency for the d_{xy}-like state as compared to that for the d_{xz}- and d_{yz}-like states, another feature in agreement with the nature of the molecular orbitals from our SCCEH investigation[15] (as indicated by the closeness of the coefficient of d_{xy} to unity in the molecular orbital expressions in Figure 3). Lastly, the parameters[33] Δ (1049 cm^{-1}) and V (606 cm^{-1}) of the crystal field theory[32] can be compared respectively with the separation (1073 cm^{-1}) between the center of gravity of the two d_{xy}- and d_{yz}-type levels and the d_{xy}-type ($d_{x^2-y^2}$ in our convention of axes) level and the separation (437 cm^{-1}) (after incorporation of the influence of spin–orbit interaction), between the d_{xz}- and d_{yz}-type levels from the SCCEH investigation.

b. Nitrosylhemoglobin. The second system for which we have investigated the g shift tensor is NOHb. This system has a number of differences from ferricyt c and therefore its study provides a valuable complement to the latter system in analyzing the theory. These differences include the fact that the unpaired electron is in a d_{z^2}-like level[34,35] in NOHb instead of a d_{yz}-like level as in ferricyt c. Secondly, as a consequence of the latter fact, the g-tensor components in NOHb are close to free-electron-like[36–39]

(20) Watson, R. E.; Freeman, A. J. In "Hyperfine Interactions"; Freeman, A. J., Fraenkel, R. B., Eds.; Academic Press: New York, 1971.

(21) Rodgers, J. E.; Lee, T.; Das, T. P.; Ikenberry, D. *Phys. Rev. A* **1973**, *7*, 51–59. Rodgers, J. E.; Das, T. P. *Ibid.* **1973**, *8*, 2195–2196.

(22) Evans, L.; Sandars, P. G. H.; Woodgate, G. K. *Proc. R. Soc. London, A* **1965**, *A289*, 108–113, 114–121.

(23) Das, T. P. In "Relativistic Quantum Mechanics of Electrons"; Harper and Row: New York, 1973.

(24) Andriessen, J.; Raghunathan, K.; Ray, S. N.; Das, T. P. *Phys. Rev.* **1977**, *B15*, 2533–2537.

(25) Hay, P. J.; Thibeault, J. C.; Hoffman, R. *J. Am. Chem. Soc.* **1975**, *97*, 4884–4899.

(26) Whitehead, M. A. In "Sigma Molecular Orbital Theory"; Sinanoglu, O., Wiberg, K., Eds.; Yale University Press: New Haven, 1970.

(27) Duff, K. J.; Mishra, K. C.; Das, T. P. *Phys. Rev. Lett.* **1981**, *46*, 1611–1614.

(28) Roothaan, C. C. J. *Rev. Mod. Phys.* **1951**, *23*, 69–89.

(29) Duff, K. J. *Phys. Rev.* **1974**, *B9*, 66–72.

(30) Johnson, K. H. *Adv. Quantum Chem.* **1973**, *7*, 143–185.

(31) Slater, J. C. In "The Self-Consistent Field for Molecules and Solids"; McGraw-Hill: New York, 1974; Vol. 4.

(32) Taylor, C. P. S. *Biochem. Biophys. Acta* **1977**, *491*, 137–149.

(33) The values of V and Δ quoted for the crystal field treatment are obtained by using the ratios $V/\lambda = 1.48$ and $\Delta/\lambda = 2.56$ from Table II of ref 32 and the spin–orbit constant $\lambda = 410$ cm^{-1} used in the present work.

(34) Mun, S. K., in ref 6.

(35) Wayland, B. B.; Olson, L. W. *J. Am. Chem. Soc.* **1974**, *96*, 6037–6041.

(36) Chien, J. C. W. *J. Chem. Phys.* **1969**, *51*, 4220–4227.

(37) Utterback, S. G., in ref 8.

(38) Doetschman, D. C.; Utterback, S. G. *J. Am. Chem. Soc.* **1981**, *103*, 2847–2852.

in contrast to ferricyt *c*. Lastly, the d-like levels carry seven electrons[34,35] with the t-type levels being all doubly occupied.

Before discussing our results for this system, we would like to briefly summarize earlier work on the **g** tensor in this system. Single crystal EPR measurements have been performed in horse-heart NOHb,[36] human NOHb,[37,38] and NO derivatives of Hb Kansas.[39] Structural data from X-ray measurements are available only[40] in horse-heart NOHb. Unfortunately, at the time that the EPR measurement[36] in horse-heart NOHb was performed, the X-ray data[40] were not available. Consequently, the orientation of the principal components with respect to the crystal axes and actually what is more meaningful to axes based on the heme system was not directly measurable. However, attempts have been made[36,37] in the literature to utilize the principal components and principal axes of the **g** tensor and the ¹⁴N hyperfine (A) tensor, associated with the NO group, to draw conclusions about the Fe–N–O bond angle and the orientations of the two principal axes systems with respect to the heme normal and N–O bond directions. In earlier interpretations[36] of horse-heart NOHb **g**- and A-tensor data, the **g**-tensor component which had the value closest to the free-electron value was considered to be oriented along the N–O bond direction. From this analysis, the Fe–N–O bond angle was found to be 110° as compared to (145° ± 10°) from X-ray data[40] on horse-heart NOHb. A subsequent analysis[37] of the data in human NOHb that does not consider the heme normal to coincide with any of the principal axes of the **g** tensor, but instead uses an empirical fit to the A- and **g**-tensor data to determine the contributions to the unpaired spin-density distribution from various Fe and N orbitals, has led to Fe–N–O bond angles of 137° and 130°, respectively, for the α and β chains and angles of 10° and 8° between the principal *Z* axis of the **g** tensor and the heme normal. There is no X-ray information on the Fe–N–O bond angles in human NOHb, but the corresponding angle[40] of 145° ± 10° in the horse-heart system is in reasonable agreement with the Fe–N–O bond angles in human NOHb from the latter analysis.

For our analysis of the **g** tensor using the procedure described in section II, we have used the electronic wave functions for the R-state of NOHb which had been obtained for our earlier investigations[34] of the ¹⁴N hyperfine interactions in this system and which corresponds to the situation for which the **g** tensor has been reported in the literature for human and horse-heart NOHb. The Fe–N–O bond angle in our earlier work[34] had been taken as 145° from a consideration of the structures of five[41] and six[42] liganded nitrosyl–heme systems. Since this bond angle is the same as that[40] in horse-heart NOHb, we can consider our work to be representative of the horse-heart NOHb system and we should make comparisons between our theoretical results and the experimental results for the latter system.[36] However, there are differences in the azimuthal angle for the N–O bond for the model system we have used and the corresponding angles[40] of 205° and 195°, respectively, for the α and β chains of horse-heart NOHb. The azimuthal angle for our model system[34] is 225°, corresponding to the NO group directly above the Fe–N₃ line (Figure 2), the Fe atom being on the porphyrin plane in the R state. The possible influence of this difference in azimuthal bond angles on the components g_{xx} and g_{yy} of the **g** tensor will be discussed when we consider the reusutls of our investigation later in this section.

The contributions to the components of the **g** tensor in NOHb were obtained as in the case of ferricyt *c* with eq 11 in section II. The difference between the present case and ferricyt *c* is that with seven electrons in d-like states, the unpaired electron is now[34] in a d_{z^2}-like state, which provides a satisfactory explanation of the ¹⁴N hyperfine interaction data in this system.

The consequence of this situation is that in contrast to the case of ferricyt *c*, the unpaired spin distribution is nearly axially

symmetric about the *Z* direction, perpendicular to the heme plane, as in Figure 2, and so the **g** tensor is expected to be close to free-electron-like. However, there is some departure from axial symmetry due to the inclination of the NO direction to the *Z* axis, and there is some mixing of the d orbitals of different symmetry in the occupied and unoccupied molecular orbitals. This would lead to some departure from free-electron character through the perturbation term in eq 11, especially for the g_{xx} and g_{yy} components and also to finite off-diagonal components for **g** tensor. However, these effects are expected to be rather small compared to the case of ferricyt *c*, because the energy difference involved for excitations of the type in Figure 1b is much larger than in the former system, where the unpaired spin electron was in a d_{xz}-like state close to the paired d_{yz}-like state (Figure 3). These features are borne out by the **g** tensor in the molecular axis system in eq 16:

$$\hat{g} = \begin{pmatrix} 2.0023 & -0.0018 & 0.0000 \\ -0.0018 & 2.0351 & 0.0000 \\ 0.0000 & 0.0000 & 2.0345 \end{pmatrix} \qquad (19)$$

the designations of the columns and rows in eq 16 being the same as in eq 13. The g_{zz} component is close to free-electron-like because the unpaired spin–orbital is almost completely axially symmetric, making the contributions from the perturbation term in eq 11 nearly zero. The contributions from the perturbation term for all the other components of the **g** tensor arise primarily from excitations of the type in Figure 1b. Additionally, for all of these terms, close to 15% of contribution arises from excitations of the type (1b) from low-lying paired spin levels with primarily ligand orbital characters but also from some significant d characters to the d_{z^2}-like level which contains the unpaired spin electron. This type of contribution would be missed if one used a crystal-field model. On diagonalizing the **g** tensor in eq 19, we get the principal components and direction cosines for the principal axes given in eq 19 and 20, the conventions for the latter being the same as in eq 15 for ferricyt *c*.

$$g_{z'z'} = 2.0023, \ g_{x'x'} = 2.0352, \ g_{y'y'} = 2.0345 \qquad (20)$$

$$\gamma_{i'i} = \begin{pmatrix} 0.9985 & -0.0548 & 0.0000 \\ 0.0548 & 0.9985 & 0.0016 \\ 0.0000 & -0.0016 & 0.9999 \end{pmatrix} \qquad (21)$$

The principal components of the **g** tensor for horse-heart hemoglobin[36] with which our results can be compared are 1.9909, 2.0254, and 2.0824, respectively, at liquid nitrogen temperature. The overall agreement between these values and ours in eq 20 is quite good. The smallest component is almost exactly free-electron-like and from eq 21, the principal axis corresponding to it appears about 3° away from the heme normal, not very different from the values 8° and 10° for α and β chains in human NOHb derived from the parametric analysis[37] of **g** tensor and A-tensor data discussed earlier.

The one aspect of the experimental data[36] that is in significant disagreement with our results in eq 20 is the difference between the principal components $g_{x'x'}$ and $g_{y'y'}$. To a lesser extent, there is also the feature that the experimentally observed departures $\delta g_{x'x'}$ and $\delta g_{y'y'}$ of the $g_{x'x'}$ and $g_{y'y'}$ components from free-electron value are significantly larger, percentage wise, than the results of our theoretical analysis. Considering the components of the nondiagonal form of the **g** tensor in eq 16, especially the g_{xx} and g_{yy} components because they make the major contributions to $\delta g_{x'x'}$ and $\delta g_{y'y'}$, it appears that one could get an increase in these departures through either an increase in the numerator in the perturbation term in eq 11 or a decrease in the denominator. For the former it would be necessary to have the d-like orbitals have more Fe 3d character and hence larger spin density on Fe than the presently obtained result close to 65%. This would diminish the spin transfer to the ligand nitrogen atoms, especially the nitrosyl and N_ϵ atom of the proximal imidazole, which are responsible for the observed ¹⁴N hyperfine splittings in the EPR spectra[36-39] and thus destroy the reasonable agreement between theory[34] and experiment.[36-39] The other possibility is a decrease in the energy separations of the d_{xz}- and d_{yz}-like levels with respect

(39) Chien, J. C. W.; Dickinson, L. C. *J. Biol. Chem.* **1977**, *252*, 1331–1335.

(40) Deatherage, J. F.; Moffat, K. *J. Mol. Biol.* **1978**, *134*, 401–417.

(41) Piciulo, P. L.; Rupprecht, G.; Scheidt, W. R. *J. Am. Chem. Soc.* **1974**, *96*, 5293–5395.

(42) Scheidt, W. R.; Frisse, M. E. *J. Am. Chem. Soc.* **1975**, *97*, 17–21.

to the d_{z^2}-like which would diminish the denominators of the perturbation terms in eq 12 making major contributions to δg_{xx} and δg_{yy} which are of the type in Figure 1b and hence enhance the departures from free-electron character. However, with this explanation, to explain the significant observed asymmetry[36] in $g_{x'x'}$ and $g_{y'y'}$, one would have to assume the d_{xz}-like level to be significantly higher than the d_{yz}-like level. This could be the result of the asymmetric observed[40] disposition of the NO bond in horse-heart NOHb in contrast to the symmetrical situation[34] we have used. This possibility should be tested in the future, but it is also possible that there may be some asymmetry produced in the electron distribution due to the interaction between some groups on the protein chain and the heme unit, as pointed out for ferricyt c, section IIIa. This situation would be similar in nature to, but different in detail from, that found[43] for met Mb, where one needed an asymmetry between diagonally opposite pyrrole rings to explain asymmetries in single-crystal ^{14}N hyperfine data.[44]

To reinforce some of these conclusions, it will be worthwhile to carry out, as in the case of ferricyt c, perturbation calculations of the present type with wave functions and energy levels from more first-principle calculations, such as by the Hartree–Fock procedure[27-29] and the approximate MS-Xα approach.[30,31] The influence of spin–orbit interaction on the energy-level spacings is not expected to be as important a contributing factor as in ferricyt c, where the important energy difference for g_{zz}, g_{xz}, and g_{yz} was the small one between d_{xz} and d_{yz} which was very significantly influenced by spin–orbit interaction. In the present case it is the relatively large separation between the d_{z^2}-like and other levels that is involved, which is percentage-wise not as significantly

influenced by spin–orbit interaction. In this system also, it would be desirable to study the influence of other mechanisms discussed earlier for ferricyt c, particularly the exchange polarization mechanism. In this connection, one would also like to examine how well the ^{14}N hyperfine tensor for the NO group, after incorporation of exchange polarization, compares with experiment[36-39] both with respect to the magnitudes of the principal components and the orientations of the principal axes. In particular, it would be interesting to see if one of the principal components of the **A** tensor does, in fact, coincide with or lie close to the NO bond direction as has been assumed in earlier empirical analysis[36] for determination of the Fe–N–O bond angle.

IV. Conclusion

The investigations reported in the present work for two low-spin hemoglobin derivatives indicate that the perturbation approach for the **g** tensor with molecular orbital wave functions and energy levels provides reasonable overall agreement with experiment and can therefore be used as a check on the electronic charge and spin distributions over hemoglobin derivatives, which can complement their hyperfine properties in this respect. Since this procedure directly uses the wave functions and energy levels from electronic structure investigations and does not use any parametric fits to experimental data, the comparison of the results with experiment can be used to draw conclusions regarding improvements in the calculated electronic structure and other mechanisms contributing to the **g** tensor. Two such mechanisms are discussed and the role of one of them, the exchange polarization mechanism, is emphasized. It is hoped that similar investigations, as in the present work, of additional low-spin hemoglobin derivatives will be carried out in the future to test the general applicability of the conclusions obtained here.

Registry No. ferricyt c, 9007-43-6.

(43) Mishra, K. C.; Mishra, S. K.; Scholes, C. P.; Das, T. P. J. Am. Chem. Soc. **1983**, 105, 7553–7556.
(44) Scholes, C. P.; Lapidot, A.; Mascarenhas, R.; Inubushi, T.; Isaacson, R. A.; Feher, G. J. Am. Chem. Soc. **1982**, 104, 2724–2735.

Structural Dependence of the Singlet–Triplet Energy Gap of the Tetramethylene Biradical

C. Doubleday,*† J. McIver,*‡ and M. Page§

*Contribution from the Department of Chemistry, Columbia University,
New York, New York 10027, the Department of Chemistry, State University of New York at
Buffalo, Buffalo, New York 14214, and the Laboratory for Computational Physics, Naval
Research Laboratory, Washington, D.C. 20375. Received May 8, 1985*

Abstract: Ab initio calculations were performed on the tetramethylene biradical with use of a 2-configuration MCSCF wave function and the 3-21G basis set. The singlet–triplet energy gap E_{ST} was calculated as a function of the three internal rotation angles, both with planar sp^2 terminal methylene groups and with pyramidal terminal methylenes. Over most of the surface through-bond coupling dominates E_{ST}, and for certain symmetric structures this effect is analyzed. With regard to the intersystem crossing process, the important result is the extraordinary ease with which singlet–triplet intersections are encountered during the lifetime of the triplet biradical.

Triplet 1,4-biradicals are now familiar reactive intermediates in organic chemistry.[1] Despite the familarity, we have only a rudimentary understanding of their lifetimes and product distributions. This is not surprising in view of the complexity of the intersystem crossing (isc) problem. A major hindrance to investigators has been the absence of any firm knowledge of the relation between biradical structure and the singlet–triplet (S–T) energy gap.

A complete theoretical description of isc in 1,4-biradicals is currently intractable. Certainly, the least one requires is the location of important regions of the S–T intersection hypersurface, and the present calculations are directed toward that goal. While this still leaves us far from the ultimate goal of calculating the isc rate constant a priori, the location of the S–T intersection places

(1) (a) Wagner, P. J. Acc. Chem. Res. **1971**, 4, 168. (b) Wagner, P. J. In "Rearrangements in Ground and Excited States"; deMayo, P., Ed.; Academic Press: New York, 1980; Vol. 3, pp 402–439. (c) Platz, M., Ed. Tetrahedron **1982**, 38 (6), 733–867. (d) Dervan, P. B.; Dougherty, D. A. In "Diradicals"; Borden, W. T., Ed.; Wiley: New York, 1981; pp 107–149. (e) Engel, P. S. Chem. Rev. **1980**, 80, 99.

†Columbia University.
‡State University of New York at Buffalo.
§Naval Research Laboratory.